Supplement to: Mineralogy and mixing state of North African mineral dust by on-line single-particle mass spectrometry.

S1 Dispersed soil dust properties.

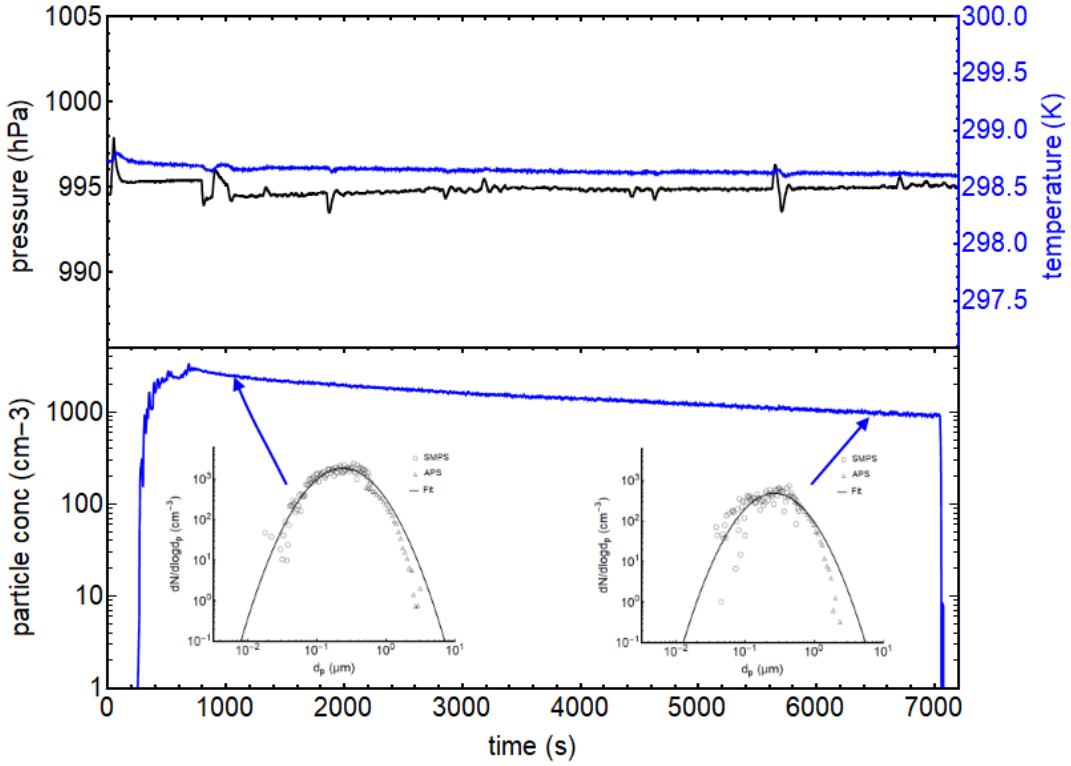

Figure 1. Time series of an experiment in the APC after the injection of dust sample DDS02, showing the pressure and temperature (upper panel) and the aerosol number concentration measured with a Condensation Particle Counter (CPC, lower panel). Also in the lower panel, the size distribution from combined Scanning Mobility Particle Sizer (SMPS, circles) and Aerodynamic Particle Sizer (APS, triangles) measurements are shown for two times during sampling. The mobility and aerodynamic diameter was converted to a volume-equivalent diameter. The solid lines show the lognormal function fit.

S2 Cluster analysis methods

Large quantities of unique spectra are produced by SPMS that must be organised into composition classes for interpretation. Cluster analysis techniques classify particles on the basis that similar mass spectral patterns are produced by particles of similar composition. The outcome of the analysis can be affected by the choice of clustering algorithm and the pre-processing of the raw data (Rebotier and Prather, 2007), which should be considered when interpreting the data. In addition, instrument design features, such as ablation laser wavelength, can result in different spectral patterns for similar particle types (Hinz et al., 2006), so that some caution must be applied when comparing the results from one single particle mass spectrometer with those of another. For this study, we utilised the fuzzy c means algorithm that is provided in the LAAP-TOF Data Analysis software (v 1.0.2) provided by the original equipment manufacturer (AeroMegt GmbH).

In bipolar TOF data, each particle is described by both positive and negative ion stick spectra which are combined into a single matrix before the algorithm is applied. Stick spectra present each unit mass (0-300) as a value that is proportional to the detector response integrated over the bin width (1m/z), and is equivalent to, but not identical to the peak area of an ion species of a specific nominal mass in the raw mass spectra. Accurate representation of the raw mass spectra as stick spectra

with this method requires accurate calibration of individual spectra and sufficient resolving power to separate adjacent peaks. In addition, the dynamic range of the detector system influences the sticks spectra representation due to detector saturation and peak broadening.

The partitioning of the sea salt particles into different clusters was strongly influenced by the relative abundance of the positive ions K^+, Na^+ and $NaCl^+$, which maybe a function of particle size and the amount of absorbed water, so is not necessarily a marker of the chemistry of the particles. In addition, the positive ion stick spectral patterns are adversely affected by peak shifting and peak broadening that reduces the mass calibration accuracy and resolution below the 1Da limit required for accurate binning of the raw data signal. This results in the creation of cluster classes that are defined by the differences in the positive ion calibration rather than true differences in composition. In order to reduce the impact of these effects, cluster analysis was performed on negative ion spectra only (Analysis 2) in addition to cluster analysis with the combined positive and negative ion matrix (Analysis 1).

Fuzzy c means clustering is a soft clustering method that measures the degree of similarity, or membership coefficient (μ) that each particle has to an evolving set of cluster centres. The validity of cluster centres produced by the analysis is a complex consideration and is influenced by the user-defined parameters such as number of clusters, the required convergence to terminate the algorithm, and the fuzzyfier parameter which controls the degree of freedom a data point has to belong to other cluster centres. There is some degree of uncertainty in the fuzzy c-means clustering solution that relates to how well each cluster centre represents the real particle composition type and the false classification of individual particles into a group. In this study, we have relied on a detailed familiarity with the spectral patterns in the raw data to evaluate how representative the cluster centres were of the particle population. The minimum number of clusters was chosen that resulted in a set of clusters centres that were reproducible over several iteration of the algorithm. This turned out to be 12 cluster centres for both the analysis of the bipolar data (Analysis 1) and the analysis of the negative ion spectra only (Analysis 2). Graphical representation of the all cluster classes can be found in the supplement. With a 12 cluster solution, it was necessary to combine several cluster centres represented the same composition type.

S3 Cluster analysis Results

The LAAP-TOF single particle mass spectrometer was operated almost continuously from 4th to 22nd of August 2015 from the aerosol laboratory, during which size resolved composition was measured for 250000 individual particles. Four particle composition types were recognised in the mass spectra acquired over the sampling period. These are divided into compositional classes depending on the analysis method employed. The major particle types were; sea-spray aerosol (SSA), silicate mineral dust, calcium chloride, and secondary material. The particle number fraction of these composition classes, as determined by clustering of positive and negative spectra (Analysis 1) and negative spectra only (Analysis 2) are displayed in Figure 2. In each case, the number of classes was reduced from the original 12 class solution by combining classes of similar composition as determined by the evaluation of the cluster centre.

Overall, the two cluster analysis methods produced similar fractions of SSA (88-90%) and non-SSA particle types. The dominance of the SSA types as determined by LAAP-TOF may be a result of instrument detection and ablation efficiency that results in a bias towards certain particle types. The four major compositional types were identified using both Analysis 1 and Analysis 2 clustering methods, but the quality of the positive ion mass spectra prevented the further discrimination of unique particle classes due to the effects discussed in the method section. Removing the positive ion spectra (Analysis 2) resulted in a better differentiation of internal mixing state of aged sea salt aerosol by identifying distinct nitrate rich and sulphate rich SSA particles and also identified an organic rich secondary particle type.

For Analysis 1, 7 original classes were combined into the aged sea salt category on the basis that the major differences were caused by the peak shifting and detector saturation in the positive ion spectra. For Analysis 2, the aged sea salt class category is the combination of 3 original classes and the fresh sea salt category is the combination of 3 original classes

whose major differences are in the relative NaCl molecular ion intensities. A description of all classes and how they were combined into compositional types can be found in the supplement. A detailed description of the mass spectral properties of the Sea Spray Aerosol, silicate, calcium and secondary aerosol composition types is given in the following sections.

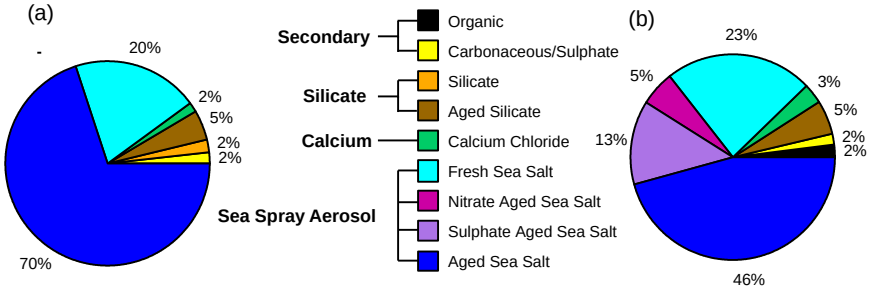

Figure 2. Particle number fractions of particle composition types determined by fuzzy c-means clustering of (a) Analysis 1, positive and negative spectra and (b) Analysis 2, negative spectra only. See text for details.

S3.1 Silicate Mineral Dust

The aluminosilicates are the most abundant rock forming minerals and form the bulk of the mineral dust in the atmosphere. Silicate particles have been identified using SPMS in laboratory and field studies using the positive elemental ion Na^+ (m/z 23), Al^+ (m/z 27), Si^+ (m/z 28), K^+ (m/z 39), and Fe^+ (m/z 56); and the negative molecular ions of SiO_2^- (m/z 60), and SiO_3^- (m/z 76) e.g (Guazzotti et al. 2001; Lee et al. 2002; Dall' osto & Harrison 2006; S. Gallavardin et al. 2008; Sullivan et al. 2006). These markers were used to identify a distinct silicate class in Analysis 1 and Analysis 2. It is noted that the reporting of a second silicate class in Analysis 1 is likely to be the result of mass calibration shift in the positive ion mass spectra. An example of a silicate class derived for Analysis 1 is displayed in Figure 3. In addition to the silicate markers, the negative mass spectra for silicate contain relatively large fragments of PO_2^- (m/z 63) and PO_3^- (m/z 79) as previously reported in SPMS analysis of surface dust collected from Cape Verde (Hinz et al., 2006) and in ambient SMPS measurements in the vicinity of the islands (Dall'Osto et al., 2010).

Atmospheric processing of the mineral dust is evident in the negative ion spectra. Markers for Cl^- (m/z -35, -37) may represent the reaction of mineral dust with HCl derived from heterogeneous reactions of sea salt with HNO_3 and H_2SO_4 (Sullivan et al., 2007b). Internal mixing of silicate with organic fragments CN^- (m/z -26) an CNO^- (m/z -42) (Hinz et al., 2006) may be a product of atmospheric processing with organic acids or be present in the original source material. Uptake of secondary nitric and sulphuric acids onto mineral dust particles result in markers for nitrate NO_2^- (m/z -46), NO_3^- (m/z -62) and sulphate SO_3^- (m/z -80), SO_4^- (m/z), HSO_4^- (m/z -97) in negative ion mass spectra of (Gallavardin et al. 2008) and is a direct indication of atmospheric aging.

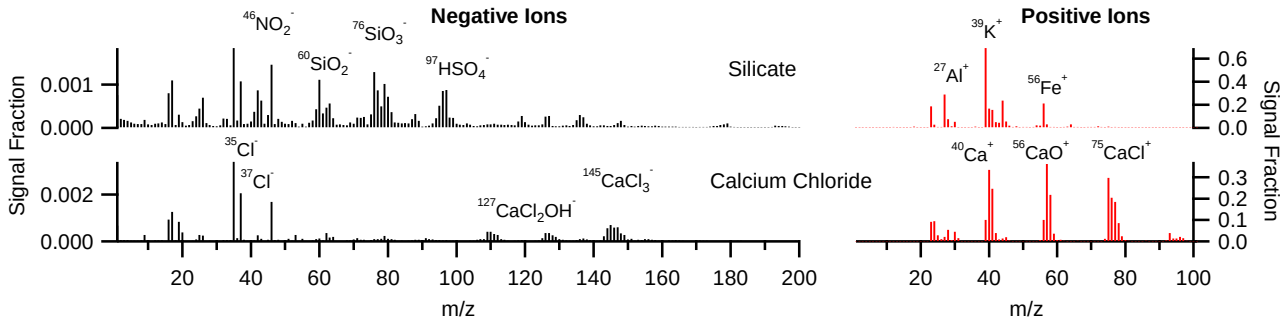

Figure 3. Stick spectra of the silicate (a) and calcium chloride (b) cluster centres produced by the fuzzy c-mean clustering of positive and negative ion spectra (Analysis 1).

S3.2 Calcium

Calcium carbonate is the most abundant non-silicate material in arid soils and is expected to be a major constituent in mineral dust aerosol. Alkaline calcium carbonate particles are expected to readily react with acid gasses in atmosphere to form calcium salts. Much attention has been given to the reaction of calcium carbonate with nitric acid to form hygroscopic $Ca(NO_3)_2$ as a mechanism to explain deliquesced calcium particle on filters (Krueger et al., 2004; Laskin et al., 2005; Matsuki et al., 2005) collected after transport through urban and industrial areas. More recently it has been suggested that in remote marine environments, the prevalence of HCl over HNO_3 favours the formation of $CaCl_2$ as the principal calcium salt (Kim and Park, 2012; Tobo et al., 2010). In this study, both Analysis 1 and Analysis 2 report a distinct calcium chloride particle class. These particles are characterised by peaks of Ca^+ (m/z 40), CaO^+ (m/z 56) and $CaCl^+$ (m/z 75, 77) in positive ion spectra and Cl^- (m/z -35, -37), $CaCl_2OH$ (m/z 127, 129, 131) and $CaCl_3$ (m/z 145, 147, 149) in negative ion spectra Figure 3(b). It is interesting to note that no evidence of $Ca(NO_3)_2$ was found in the mass spectra during this study.

S3.3 Sea Spray Aerosol

The mechanical action of wind stress on the ocean surface creates particles comprised of inorganic sea salt and organic matter which dominate the marine boundary layer (MBL) and contribute significantly to optical depth in remote marine locations (O'Dowd and de Leeuw, 2007). Primary SSA can be readily identified in SPMS by the distinctive spectral patterns created by NaCl clusters with peak of Na_2Cl^+ (m/z 81, 83) and $NaCl_2^-$ (m/z -93, -95, -97) along with abundant elemental ions of Na^+ (m/z 23), K^+ (m/z 39) and Cl^- (m/z -35, -37) (Guazzotti et al., 2001). These markers are often accompanied by negative ion marker of sulphate [SO_3^-, SO_4^- (m/z -80, -96, -97)] and nitrate [NO_2^-, NO_3^-(m/z -46, -62)] that are attributed to the uptake of secondary sulphuric and nitric acid by sea salt particles, and therefore used as a marker of atmospheric ageing in ambient SPMS studies. The presence of these sulphate and nitrate markers in SSA is therefore used to classify the particle class as aged SSA in this analysis.

Cluster analysis of negative ion spectra (Analysis 2) produced several classes of spectra featuring $NaCl_2^-$ which we attribute to SSA. Three of these classes feature varying signal fractions of Na, Cl, and combinations of Na and Cl, and no markers for atmospheric ageing. An example of one of these classes is displayed in Figure 4(a). Classes which feature markers of sulphate (m/z -80, -96, -97) and nitrate (m/z -46, -62) that are less intense than the $NaCl_2^-$ at m/z -93 are described as aged SSA. Two distinct classes of aged SSA are differentiated because of their distinct spectral patterns in which one type of aging product predominates. Nitrate aged SSA (Figure 4(c)) features nitrate conjugated with sodium, such as $NaClNO_3$ (m/z -120) and $Na(NO_3)_2$ (m/z -147), in addition to the nitrate anion markers (m/z -46, -63). Sulphate aged SSA (Figure 4(d)) contains markers of sulphates that are stronger in intensity than the $NaCl_2^-$ marker for sodium chlorine which identifies the class as SSA.

It is noteworthy that no markers of silicate were found in the SSA spectral classes, nor were markers of NaCl found in the silicate classes in any of the analysis methods. This indicates that the mineral dust and SSA are not internally mixed in a significant way. The aged SSA does contain markers of calcium sulphate $CaHSO_4$ (m/z 137) and Ca_2HSO_4 (m/z 177) (Figure 4(b)). Calcium sulphate can exist as a primary emission of gypsum from evaporite deposits in arid environments. An alternative pathway for the formation of secondary $CaSO_4$ from the reaction of NO_2 with mixtures of $CaCO_3$ and $(NH_4)_2SO_4$ has recently been demonstrated under humid conditions in the laboratory (Tan et al., 2016). However, in these MBL particles the $CaSO_4$ occurs exclusively with NaCl suggesting this calcium is a primary product of SSA and not a primary mineral emission.

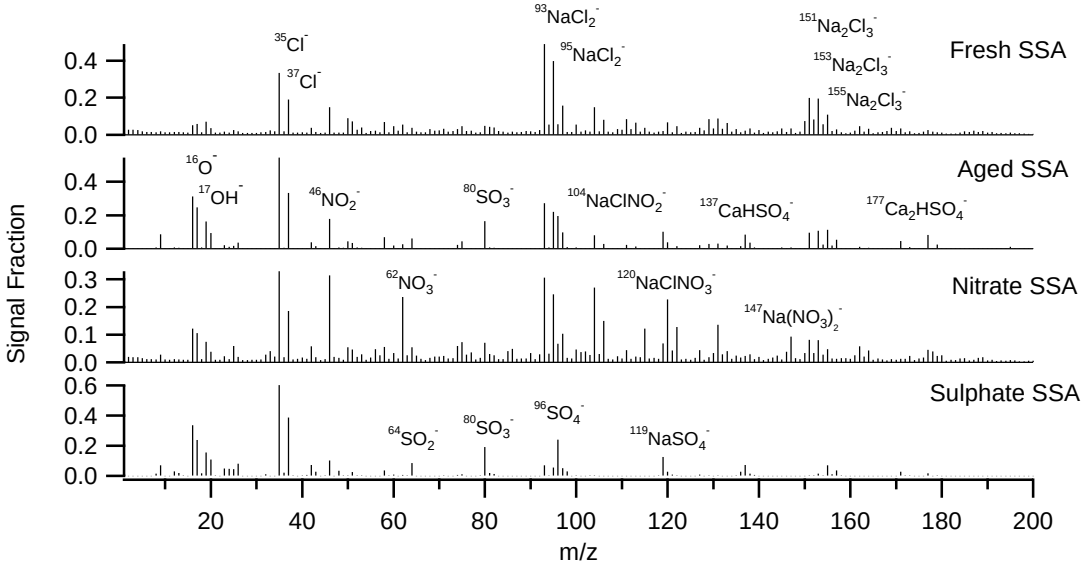

Figure 4 Stick spectra of the fresh SSA (a), aged SSA (b), nitrate aged SSA (c), and sulphate aged SSA cluster centres produced by the fuzzy c-mean clustering of negative ion spectra only (Analysis 2).

S3.4 Secondary

A class of internally mixed secondary aerosol is identified in Analysis 1 with positive ion markers of C_x^+ (m/z 12, 24, 36), NH_4^+ (m/z 18), NO^+ (m/z 30), K^+ (m/z 39), $CHNO^+$ (m/z 43) and C_2HNO^+ (m/z 55) and a negative average mass spectrum dominated by sulphate markers SO_4^- (m/z 96) and HSO_4^- (m/z 97). Cluster analysis with negative ion spectra only (Analysis 2) divided the secondary aerosol into two distinct classes indicating that the mixing state of these particles is not fully resolved by the clustering method. In Analysis 2, a secondary organic class is identified whose dominant peaks are organic markers of CN^- (m/z 26), CNO^- (m/z 42), but also contains some sulphate (m/z 96, 97). A secondary sulphate class also contains organic markers, but as minor constituents in comparison to the dominant sulphate marker peaks SO_4^- (m/z 96) and HSO_4^- (m/z 97). It is noteworthy that the secondary sulphate is the only particle class that does not contain significant amount of chlorine Cl^- (m/z 35, 37).

S3.5 Temporal evolution of external mixing state of boundary layer aerosol

Cluster time series of Analysis 2 shows a background marine aerosol population dominated by sea salt that is periodically influenced by episodes of relatively high loadings of silicate mineral dust (Figure 5). We have divided the time series into three periods separated by two distinct dust events, D1 and D2, which were selected for their distinct aerosol properties. In the pre-dust period, the non-SSA background aerosol number population is dominated by secondary sulphate particles with sporadic episodes of relatively high number concentrations of secondary organic particles that are probably of local origin. The arrival of elevated concentrations of silicate mineral dust around mid-day on 09/08/2015 defines event D1 and marks the start of an intra-dust period where the non-SSA aerosol number concentrations are influenced by fluctuating levels of silicate mineral dust. In this period, the calcium chloride time series is similar to that of silicate suggesting a common source for these particles and supporting the hypothesis that the $CaCl_2$ is formed from the atmospheric processing of terrestrial $CaCO_3$. During the inter-dust period, the number concentration of the sulphate particles declines steadily whereas the secondary organic number concentration appeared to be influenced by silicate dust concentration. The nitrate aged SSA class of particle is particularly prevalent during the intra-dust period.

An interesting period in the time series is marked by a large increase in the sulphate aged SSA around 15:00 on 17/08/2015. This shows a dramatic increase in the displacement of Chlorine in NaCl by sulphates and defines event D2 on the time series that will be referred to later in the text.

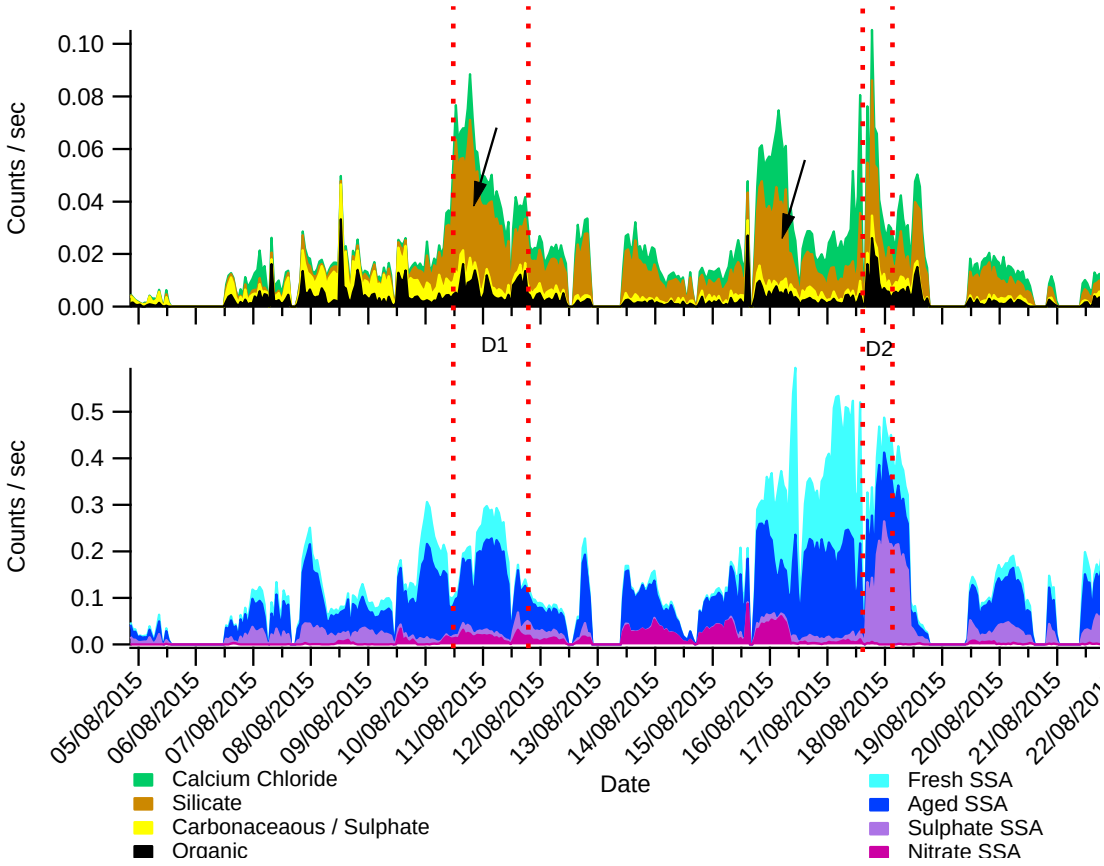

Figure 5. Stacked cluster time series of fuzzy c-means clustering using negative ion spectra only (Run 2) showing a) non-sea spray aerosol classes and b) sea spray aerosol. Dust events D1 and D2 are highlighted.

may be present.

S4 Transport History of Mineral Dust

Back trajectories for D1 and D2 (Figure 6 (a) and Figure 7 (a)) predict particle transport in the MBL with the north easterly trade winds for at least 72 hours before arrival at Praia, in agreement with previous studies of aerosol in this location during the summer (Carpenter et al., 2010; Patey et al., 2015; Salvador et al., 2016). In comparison to D2, the hourly back trajectories are more varied for D1 with the prevailing anti-cyclonic flow (Trajectories T1 and T3 Figure 6 (c)) being periodically interrupted by air masses that originate from within the African continent. The air mass back trajectory that ends at the time that roughly coincides with the peak silicate number concentration for D1 (00:30 11_08_2015 indicated by the peak detection rate of silicate particles) shows a possible influence of air mass that had been lofted to a height of 4000m over the Saharan region (Trajectory T2, Figure 5 (b,c)). Examination of the aerosol subtype product from the CALIPSO shows that a significant dust plume existed and was synchronous with the air mass trajectory at this altitude and location at 13:24 06/08/2015 (Figure 6 (d)). Furthermore, the aerosol subtype cross-section for 14:36 07/08/2015 (Figure 6 (e)) indicates significant dust in the boundary layer off the Moroccan coast at a location where the air mass back trajectories and the satellite are synchronous. Given the prevailing on-shore wind at this location, it is unlikely that this boundary layer dust originated in the coastal region of Morocco, but was transported via the collapse of a lofted SAL as indicated by the back trajectories. This hypothesis is supported by the dust model simulations for 07_08_2105 in which a significant dust plume is

indicated by the total aerosol optical thickness (AOT) from the UM Figure 6 (b), but not by the ground level dust prediction Figure 7 (a). It is noteworthy that the dust model simulation for midnight 11/08/2015 shows dust over Cape Verde (Figure 7 (c,d)) at the time of the high dust concentration measured by LAAP-TOF.

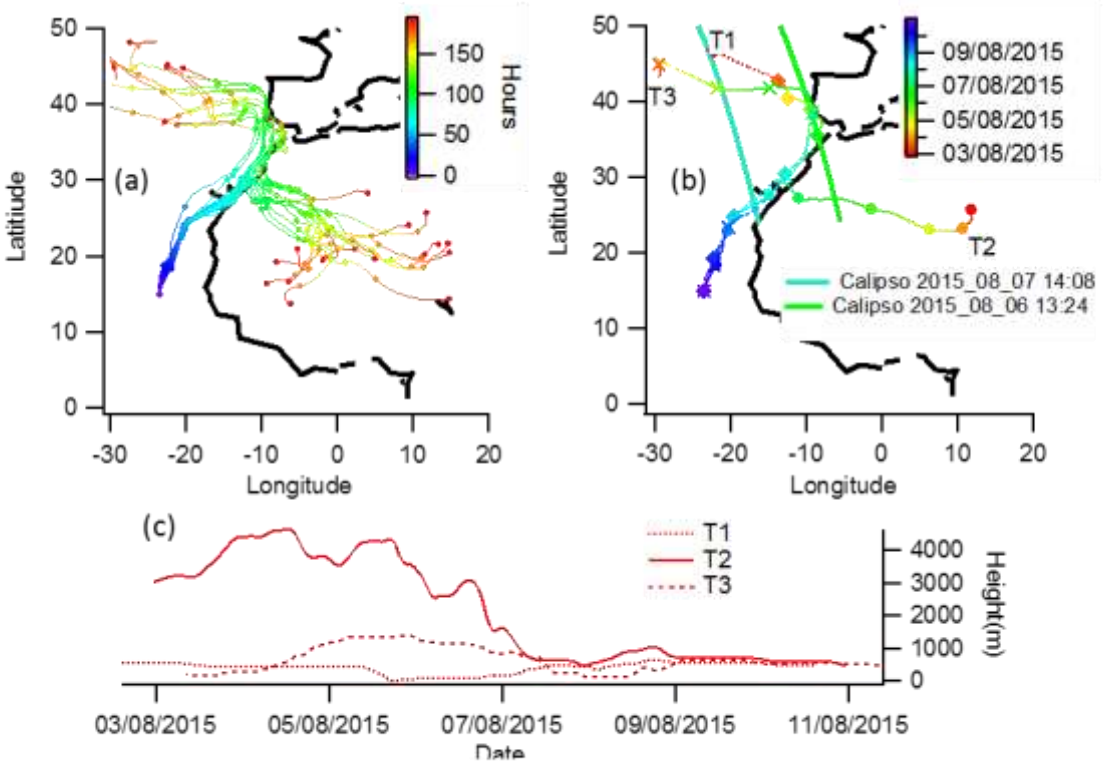

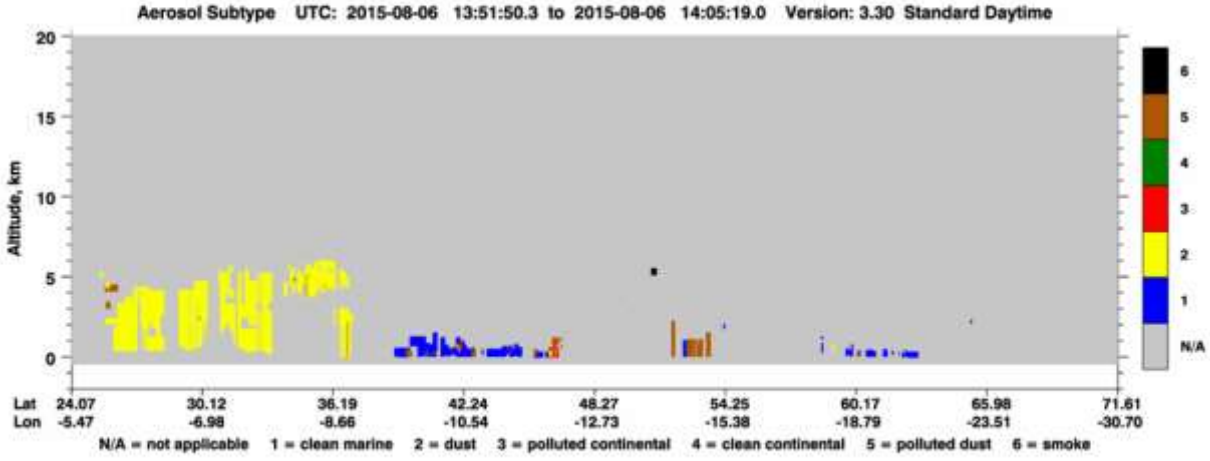

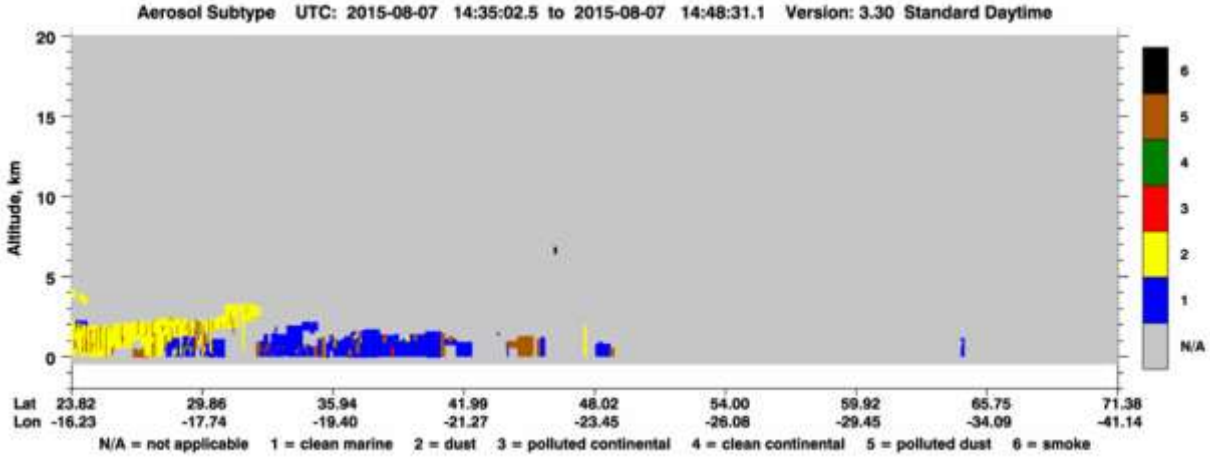

Figure 6 Air mass transport history for dust period D1. (a) 8 day (192 hour) back trajectories from the ground site at 1 hour intervals, (b) the temporal alignment of selected air mass histories (T1, T2, T3) with the overpass of the CALIPSO satellite, (c) the vertical profile of selected air back trajectories T1, T2, T3. The aerosol subtype cross-sections calculated for the CALIPSO overpasses on the 06/08/2015 and 07/08/2015 are shown in (d) and (e) respectively.

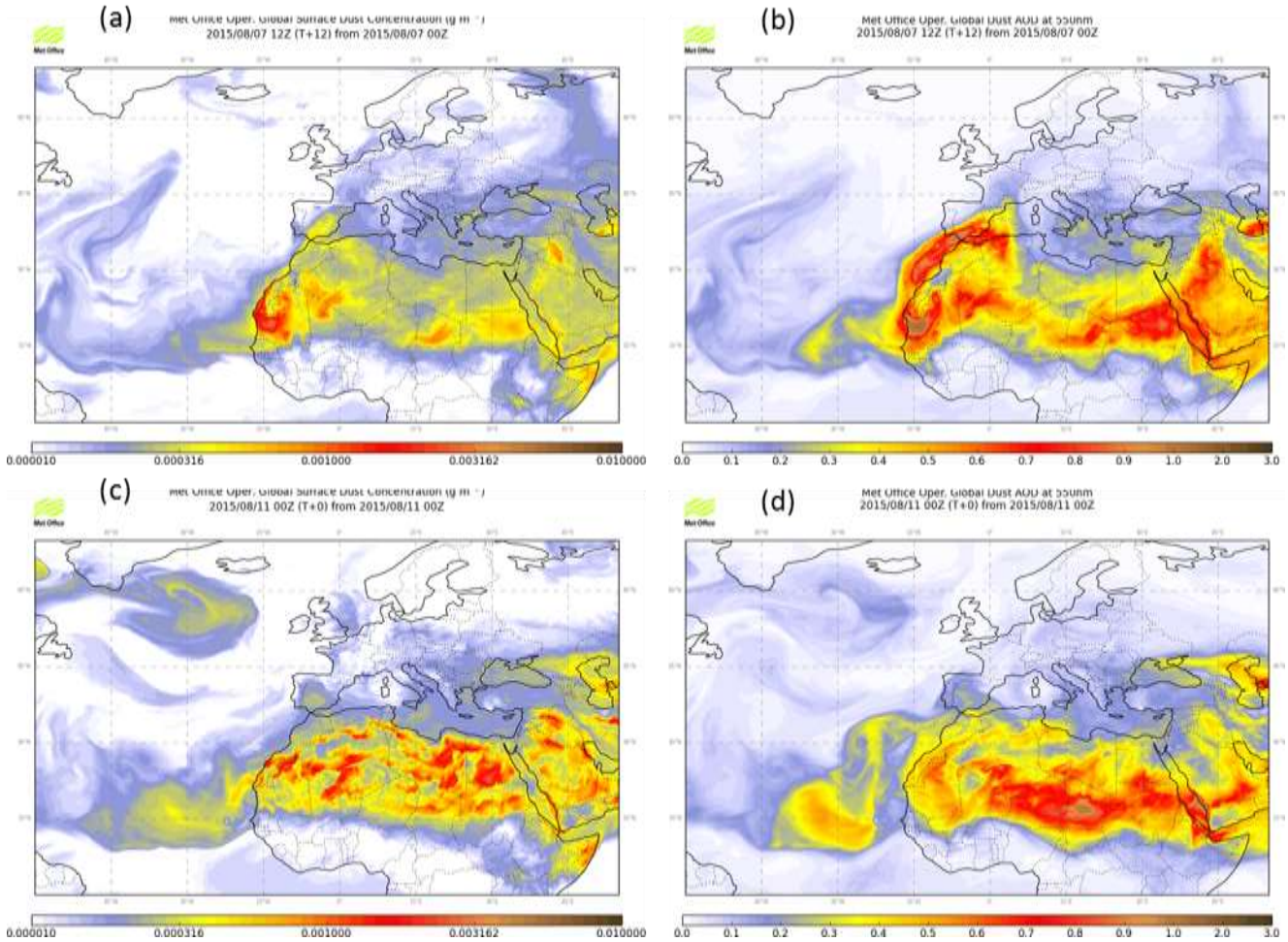

Figure 7 UM model dust product of Saharan dust for mid-day on 07_08_2015 (upper panels) and mid-night on 11_08_2015 (lower panels). Surface dust concentrations are shown on (a) and (c), and total AOD in (b) and (d).

Back Trajectories for the air mass associated with D2 indicate a more direct route for the silicate dust arriving at Praia for this period. The trade wind crosses the continental land mass in Western Sahara and Northern Mauritania (Figure 7 (a)), before crossing the ocean at low levels (Figure 7 (c)). The CALIPSO aerosol subtype product indicates an enormous dust plume extending from ground level to 7km altitude a few hundred kilometres further east (Figure 7 (d)) at the time the air mass crosses the continent 02:38 15/08/2015. At the time of D2 high dust loadings at the ground site, this dust is present above Praia as a distinct SAL at 3-6km in altitude, with small pockets of dust in the boundary layer (Figure 7 (e)).

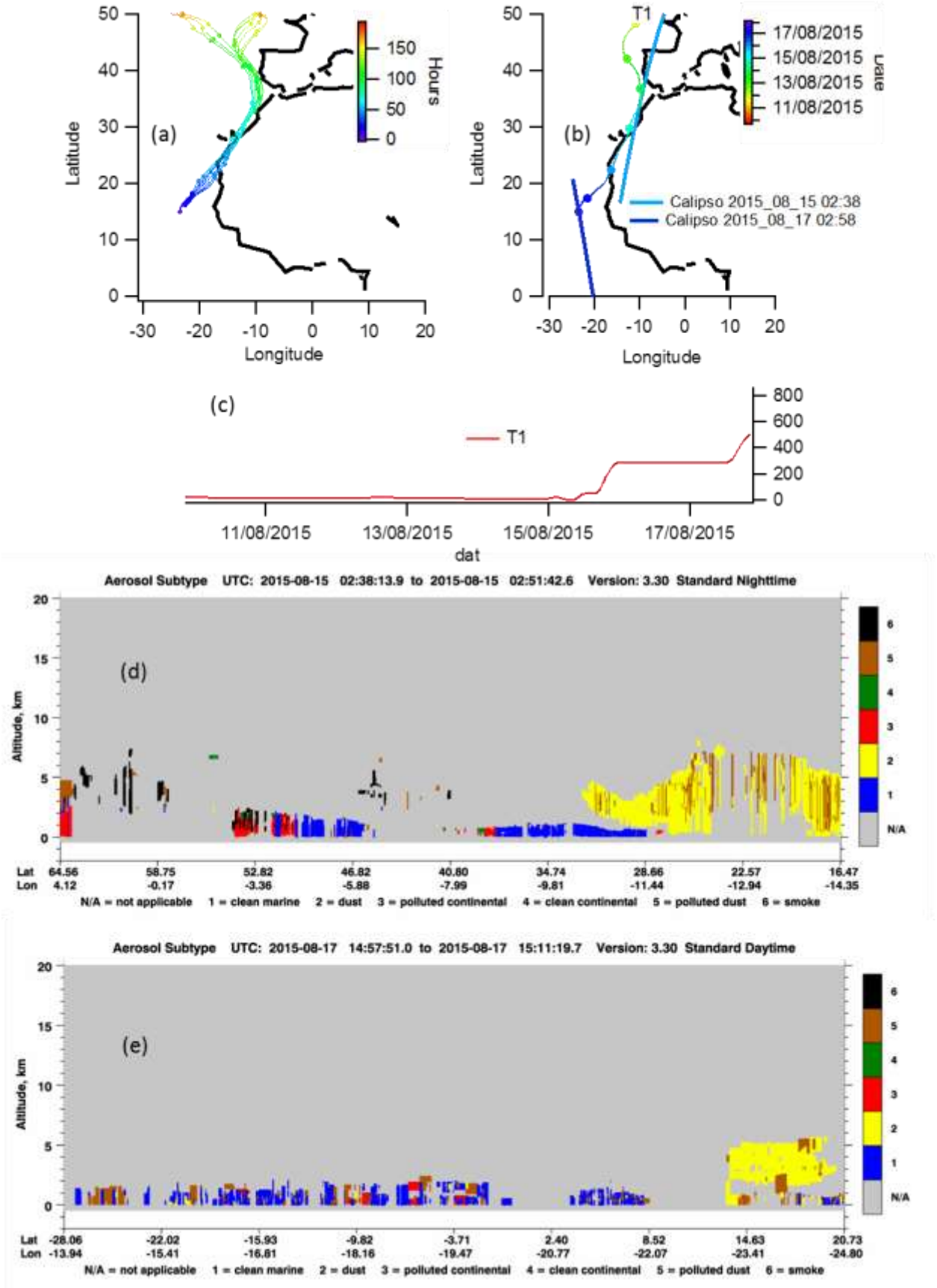

Figure 8 Air mass transport history for dust period D2. (a) 8 day (192 hour) back trajectories from the ground site at 1 hour intervals, (b) the temporal alignment of a selected air mass histories (T1) with the overpass of the CALIPSO satellite, (c) the vertical profile of selected air back trajectories T1. The aerosol subtype cross-sections calculated for the CALIPSO overpasses on the 15/08/2015 and 17/08/2015 are shown in (d) and (e) respectively.

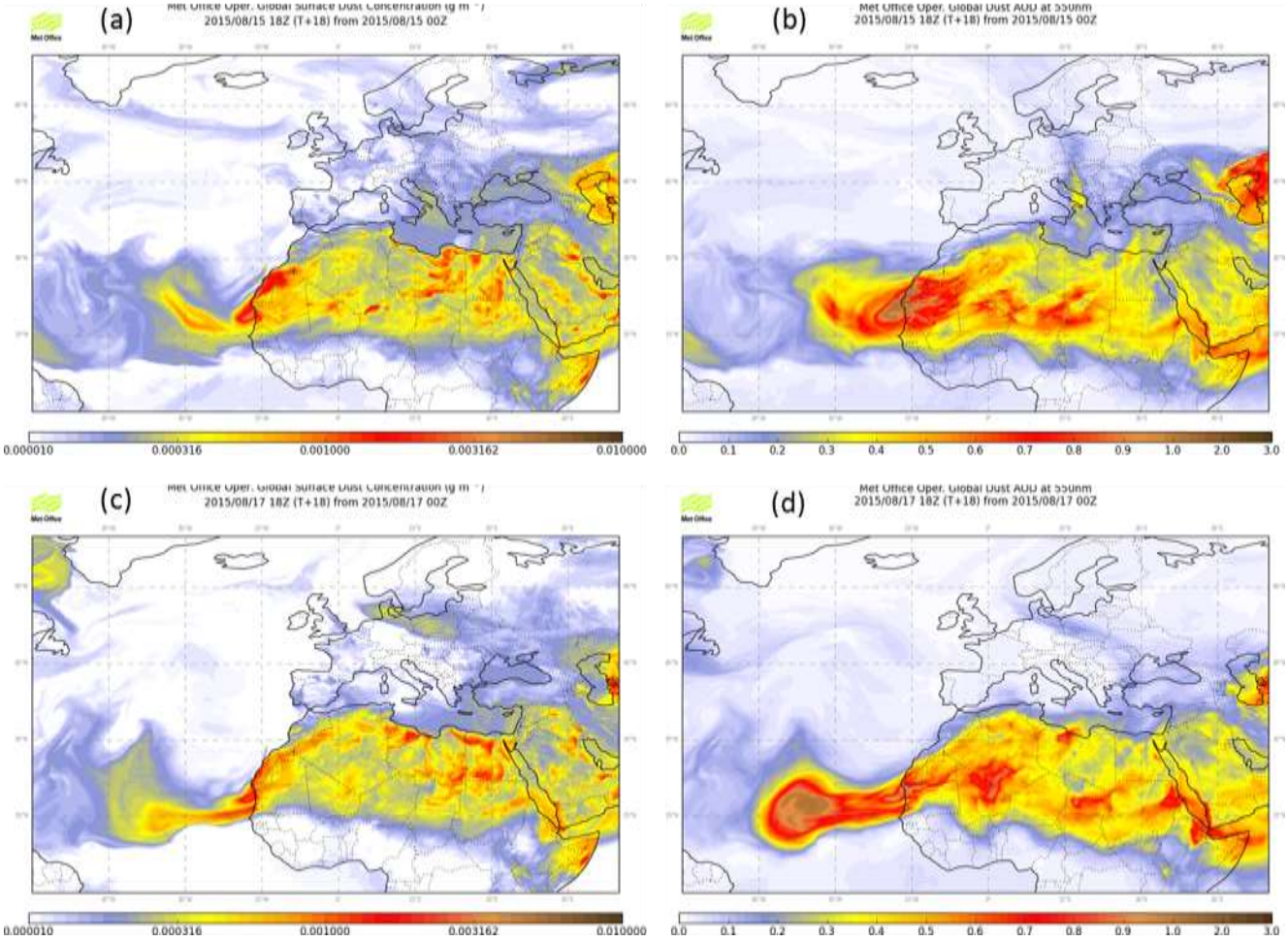

Figure 9 UM model dust product of Saharan dust for 18:00 on 15_08_2015 (upper panels) and 18:00 on 17_08_2015 (lower panels). Surface dust concentrations are shown on (a) and (c), and total AOD in (b) and (d).

S5. Satellite Imagery.

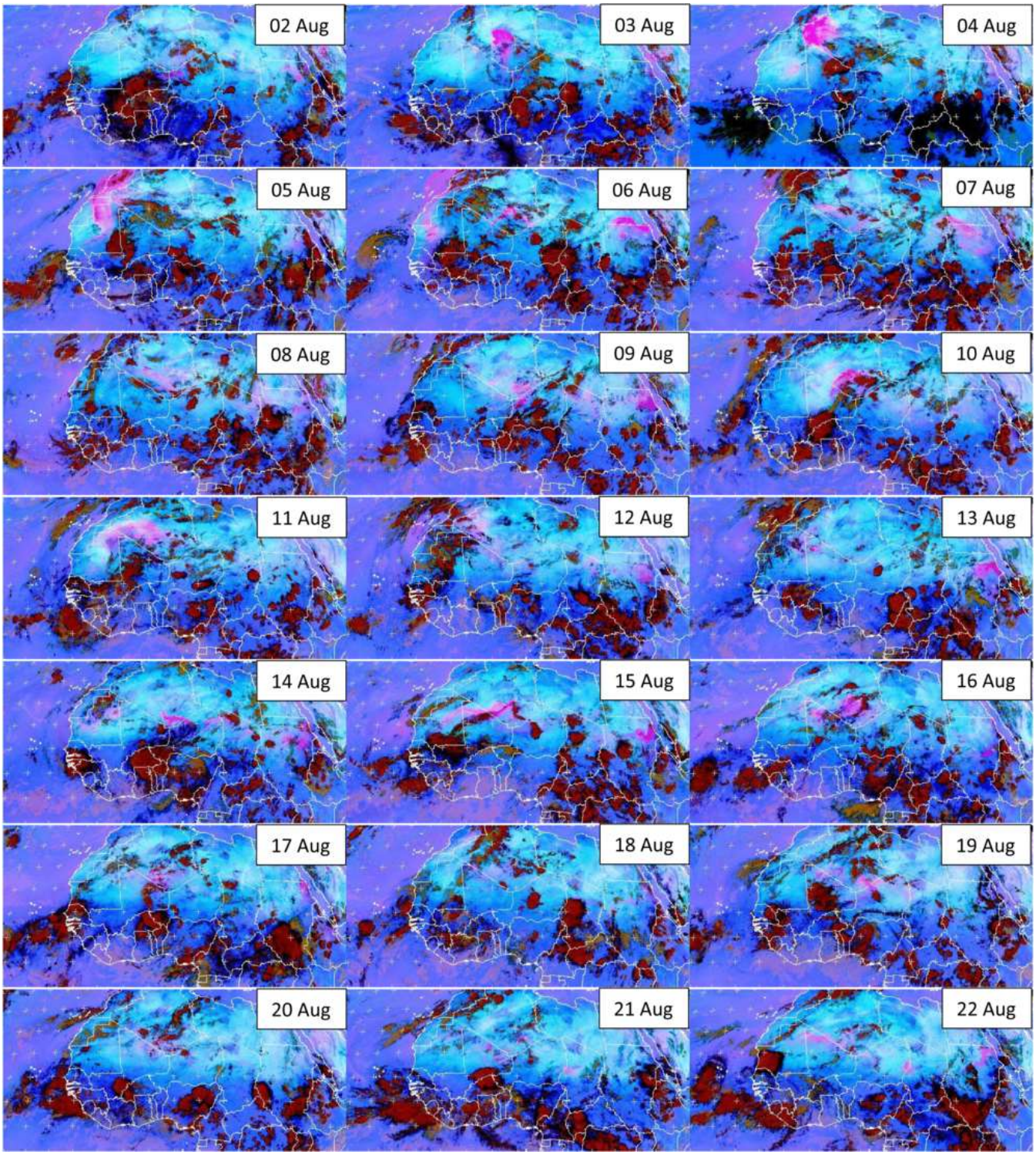

Figure 10. Satellite images from the ICE-D sampling period. Images are from 15Z except a few days without data at that time (14Z 03/08, 16Z 08/08, 16Z 19/08)

References

Carpenter, L. J., Fleming, Z. L., Read, K. A., Lee, J. D., Moller, S. J., Hopkins, J. R., Purvis, R. M., Lewis, A. C., Müller, K., Heinold, B., Herrmann, H., Fomba, K. W., Van Pinxteren, D., Müller, C., Tegen, I., Wiedensohler, A., Müller, T., Niedermeier, N., Achterberg, E. P., Patey, M. D., Kozlova, E. A., Heimann, M., Heard, D. E., Plane, J. M. C., Mahajan, A., Oetjen, H., Ingham, T., Stone, D., Whalley, L. K., Evans, M. J., Pilling, M. J., Leigh, R. J., Monks, P. S., Karunaharan, A., Vaughan, S., Arnold, S. R., Tschritter, J., Pöhler, D., Frieã, U., Holla, R., Mendes, L. M., Lopez, H., Faria, B., Manning, A. J. and Wallace, D. W. R.: Seasonal characteristics of tropical marine boundary layer air measured at the cape verde atmospheric observatory, J. Atmos. Chem., 67(2–3), 87–140, doi:10.1007/s10874-011-9206-1, 2010.

Dall'Osto, M., Harrison, R. M., Highwood, E. J., O'Dowd, C., Ceburnis, D., Querol, X. and Achterberg, E. P.: Variation of the mixing state of Saharan dust particles with atmospheric transport, Atmos. Environ., 44(26), 3135–3146, doi:10.1016/j.atmosenv.2010.05.030, 2010.

Dallosto, M. and Harrison, R.: Chemical characterisation of single airborne particles in Athens (Greece) by ATOFMS, Atmos. Environ., 40(39), 7614–7631, doi:10.1016/j.atmosenv.2006.06.053, 2006.

Gallavardin, S., Lohmann, U. and Cziczo, D.: Analysis and differentiation of mineral dust by single particle laser mass spectrometry, Int. J. Mass Spectrom., 274(1–3), 56–63, doi:10.1016/j.ijms.2008.04.031, 2008a.

Gallavardin, S. J., Froyd, K. D., Lohmann, U., Moehler, O., Murphy, D. M. and Cziczo, D. J.: Single Particle Laser Mass Spectrometry Applied to Differential Ice Nucleation Experiments at the AIDA Chamber, Aerosol Sci. Technol., 42(9), 773–791, doi:10.1080/02786820802339538, 2008b.

Guazzotti, S. a, Coffee, K. R. and Prather, K. a: Continuous measurements of size-resolved particle chemistry during INDOEX-Intensive Field Phase 99, J. Geophys. Res., 106, 28607–28627, doi:10.1029/2001JD900099, 2001.

Hinz, K.-P., Erdmann, N., Grüning, C. and Spengler, B.: Comparative parallel characterization of particle populations with two mass spectrometric systems LAMPAS 2 and SPASS, Int. J. Mass Spectrom., 258(1–3), 151–166, doi:10.1016/j.ijms.2006.09.008, 2006.

Kim, J.-S. and Park, K.: Atmospheric Aging of Asian Dust Particles During Long Range Transport, Aerosol Sci. Technol., 46(8), 913–924, doi:10.1080/02786826.2012.680984, 2012.

Krueger, B. J., Grassian, V. H., Cowin, J. P. and Laskin, A.: Heterogeneous chemistry of individual mineral dust particles from different dust source regions: The importance of particle mineralogy, Atmos. Environ., 38(36), 6253–6261, doi:10.1016/j.atmosenv.2004.07.010, 2004.

Laskin, A., Iedema, M. J., Ichkovich, A., Graber, E. R., Taraniuk, I. and Rudich, Y.: Direct observation of completely processed calcium carbonate dust particles., Faraday Discuss., 130, 453-468-517, 519–524, doi:10.1039/b417366j, 2005.

Lee, S., Murphy, D. M., Thomson, D. S. and Middlebrook, A. M.: Chemical components of single particles measured with Particle Analysis by Laser Mass Spectrometry (PALMS) during the Atlanta SuperSite Project : Focus on organic / sulfate , lead , soot , and mineral particles, , 107, 2002.

Matsuki, A., Iwasaka, Y., Shi, G., Zhang, D., Trochkine, D., Yamada, M., Yoon-Suk, K., Chen, B., Nagatani, T., Miyazawa, T., Nagatani, M. and Nakata, H.: Morphological and chemical modification of mineral dust: Observational insight into the heterogeneous uptake of acidic gases, Geophys. Res. Lett., 32(22), 1–4, doi:10.1029/2005GL024176, 2005.

O'Dowd, C. D. and de Leeuw, G.: Marine aerosol production: a review of the current knowledge., Philos. Trans. A. Math. Phys. Eng. Sci., 365(1856), 1753–74, doi:10.1098/rsta.2007.2043, 2007.

Patey, M. D., Achterberg, E. P., Rijkenberg, M. J. and Pearce, R.: Aerosol time-series measurements over the tropical Northeast Atlantic Ocean: Dust sources, elemental composition and mineralogy, Mar. Chem., 174, 103–119, doi:10.1016/j.marchem.2015.06.004, 2015.

Rebotier, T. P. and Prather, K. a: Aerosol time-of-flight mass spectrometry data analysis: a benchmark of clustering algorithms., Anal. Chim. Acta, 585(1), 38–54, doi:10.1016/j.aca.2006.12.009, 2007.

Salvador, P., Almeida, S. M., Cardoso, J., Almeida-Silva, M., Nunes, T., Cerqueira, M., Alves, C., Reis, M. A., Chaves, P. C., Artíñano, B. and Pio, C.: Composition and origin of PM10 in Cape Verde: Characterization of long-range transport episodes, Atmos. Environ., 127, 326–339, doi:10.1016/j.atmosenv.2015.12.057, 2016.

Sullivan, R. C., Guazzotti, S. A., Sodeman, D. A. and Prather, K. A.: Direct observations of the atmospheric processing of Asian mineral dust, Atmos. Chem. Phys., 7(3), 1213–1236, doi:10.5194/acpd-6-4109-2006, 2007a.

Sullivan, R. C., Guazzotti, S. a., Sodeman, D. a., Tang, Y., Carmichael, G. R. and Prather, K. a.: Mineral dust is a sink for chlorine in the marine boundary layer, Atmos. Environ., 41(34), 7166–7179, doi:10.1016/j.atmosenv.2007.05.047, 2007b.

Tan, F., Tong, S., Jing, B., Hou, S., Liu, Q., Li, K., Zhang, Y. and Ge, M.: Heterogeneous reactions of NO2 with CaCO3-(NH4)2SO4 mixtures at different relative humidities, Atmos. Chem. Phys., 16(13), 8081–8093, doi:10.5194/acp-16-8081-2016, 2016.

Tobo, Y., Zhang, D., Matsuki, A. and Iwasaka, Y.: Asian dust particles converted into aqueous droplets under remote marine atmospheric conditions, Proc. Natl. Acad. Sci., 107(42), 17905–17910, doi:10.1073/pnas.1008235107, 2010.